ACS APPLIED MATERIALS & INTERFACES

Research Article

www.acsami.org

Novel Graphene Foam Composite with Adjustable Sensitivity for Sensor Applications

Yarjan Abdul Samad,[†,§] Yuanqing Li,[†,§] Saeed M. Alhassan,[‡] and Kin Liao*[,†]

[†]Department of Mechanical Engineering, Khalifa University of Science Technology and Research, Abu Dhabi 127788, United Arab Emirates

[‡]The Petroleum Institute, Abu Dhabi 2533, United Arab Emirates

Supporting Information

ABSTRACT: In this study, free-standing graphene foam (GF) was developed by a three-step method: (1) vacuum-assisted dip-coating of nickel foam (Ni−F) with graphene oxide (GO), (2) reduction of GO to reduced graphene oxide (rGO), and then (3) etching out the nickel scaffold. Pure GF samples were tested for their morphology, chemistry, and mechanical integrity. GF mimics the microstructure of Ni−F while individual bones of GF were hollow, because of the complete removal of nickel. The GF-PDMS composites were tested for their ability to sense both compressive and bending strains in the form of change in electrical resistance. The composite showed different sensitivity to bending and compression. Upon applying a 30% compressive strain on the GF-PDMS composite, its resistance increased to ∼120% of its original value. Similarly, bending a sample to a radius of 1 mm caused the composite to change its resistance to ∼52% of its original resistance value. The relative change in resistance of the composite by an applied pressure/strain can be tuned to considerably different values by heat-treating the GF at different temperatures prior to infusing PDMS into its scaffold. Upon heat treating the GF at 800 °C prior to PDMS infusion, the GF-PDMS demonstrated ∼10 times better sensitivity than the untreated sample for a compressive strain of 20%. The composite was also tested for its ability to retain a change in electrical resistance when a brief load/strain is applied. The GF-PDMS composite was tested for at least 500 cycles under compressive cyclic loading and showed good electromechanical durability. Finally, it was demonstrated that the composite can be used to measure human blood pressure when attached to human skin.

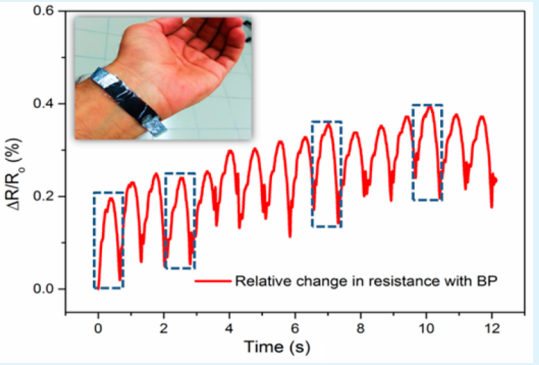

KEYWORDS: *graphene oxide, piezoresistivity, reduced graphene oxide, graphene foam, tunable piezoresistivity*

INTRODUCTION

In order to realize future robots with sensibilities comparable to those of human beings, the development of materials and fixtures with human-like sensitivity is essential.[1] Also, from the inevitable escalating demand for renewable and sustainable energy resources to stringent health monitoring, electronic materials that are stretchable and wearable have an array of applications in a variety of related current and coming-of-age technologies.[2]

Although there have been considerable works on developing artificial nose for sensing smells, touch-like human sensibilities have been very challenging to emulate.[3−5] It is intuitive to think that pressure and strain sensitivities to touch are close in principle; nonetheless, it is still a challenge to develop sensors capable of differentiating different stimuli and response to very low pressures or strains. Recently substantial advances have been made in materializing the touch sensibility through pressure-sensing mechanisms using state-of-the-art technologies and advanced nanostructured and microstructured materials and devices.[2,5−10]

Along with several sophisticated materials used in flexible and stretchable electronics, graphene, being one of today's marvel materials, has also been investigated for its usefulness in such devices.[11−15] Since the successful realization of two-dimensional (2D) graphene, it has been desired to explore its connected, three-dimensional (3D) structure to exploit its extraordinary thermal and electrical properties for different applications.[16−18] First, such graphene foam (GF) materials were proposed to be made via a few theoretical models and later were successfully realized in several experimental studies, using both chemical vapor deposition (CVD)-grown graphene and reduced graphene oxide (rGO).[19−25] Graphene is semimetallic or semiconducting in nature with a finite resistance; its 3D structures change resistance when perturbed by a local stimulus, such as local changes in temperature or electromagnetic field and an outside stimulus such as an external force;[11,26,27] and there have been several studies that have attempted to use CVD-grown and chemically modified GF materials as pressure sensors.

Received: February 19, 2015
Accepted: April 14, 2015
Published: April 14, 2015

DOI: 10.1021/acsami.5b01608
ACS Appl. Mater. Interfaces 2015, 7, 9195−9202

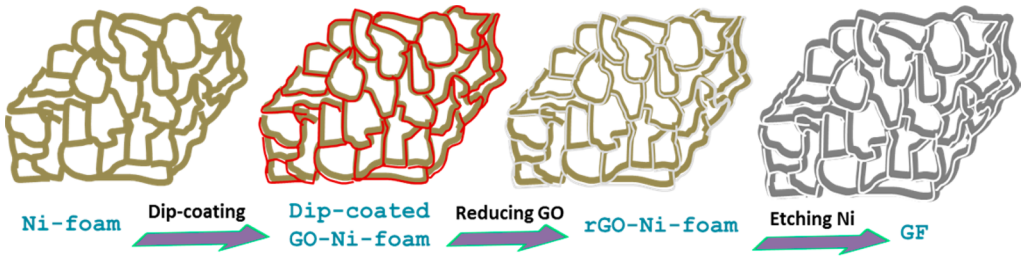

Figure 1. Schematic representation of formation of the GF.

Chen et al. developed a pioneering method of not only creating the first CVD-grown GF but also a GF-PDMS (where PDMS = polydimethylsiloxane) composite, and they have investigated its performance as a pressure/strain sensor with altered sensitivities, in response to applied tension and bending.[20] The composite was demonstrated to be perfectly reusable for 5000 cycles. In other works, mechanically robust and highly flexible chemically modified GF were directly tested for their pressure sensitivity in compression.[21,28] Yao et al. fabricated a flexible hybrid GF-polyurethane (PU) foam with pressure sensitivities ranging from 0.001 to 0.26 KPa^{-1} under compressive loads.[29] More recently, GF made from a pyrolysis method, was mixed with PDMS and tested for pressure sensitivity in bending and stretching.[30] Flexible and stretchable electronic materials and devices can be realized straightforwardly and economically using some of the aforementioned works on GF-based pressure-sensing materials.[29,31]

Although nickel foam has been previously used as a template for making GF as discussed earlier, all those methods employ a CVD technique for depositing graphene on nickel skeleton. The nickel, from the graphene-coated nickel foam via the CVD method, is removed by first protecting the graphene with poly(methyl methacrylate) (PMMA) and then etching out the nickel foam with boiling hydrochloric acid (HCl). Herein, we report another complementing work on developing a GF-PDMS-based composite as a pressure and strain sensor. We have made GF via a simple method of coating open-cell nickel foam (Ni−F) with graphene oxide (GO) by vacuum-assisted dip-coating and subsequently reducing the GO to rGO and removing the nickel skeleton by etching with boiling HCl. Later, PDMS was infiltrated inside the GF skeleton through vacuum infiltration to form a stretchable and flexible GF-PDMS composite. The composite was then tested for its pressure sensitivity under bending and compressive loads besides mechanical and microstructural analysis. The composite is sensitive enough to be used to measure human blood pressure when attached to skin. Our fabrication method for GF is inspired by the CVD-grown GF; nonetheless, it is much more facile than the latter as a simple dip-coating method is being used and, unlike the CVD-grown GF, the current method does not require any protective coating while etching the nickel.

EXPERIMENTAL SECTION

Materials. Graphite powder with a particle size of 20 mm, concentrated sulfuric acid (H_2SO_4, 98%), potassium persulfate ($K_2S_2O_8$), phosphorus pentaoxide (P_2O_5), sodium nitrate ($NaNO_3$), hydrochloric acid (HCl), potassium permanganate ($KMnO_4$), ethanol, and hydrogen peroxide (H_2O_2), hydroiodic acid (HI) were obtained from Sigma−Aldrich Co., Ltd. A silicone elastomer kit (SYLGARD 184) was obtained from SYLGARD Co., Ltd. Ni−F (90 PPI) was obtained from a local supplier (Laboratory Scientific Supplies FZC). All of the materials were directly used without further purification.

Preparation of GO Sheets. GO sheets were synthesized using the modified Hummer's method reported in our previous works and also elsewhere.[32,33]

Preparation of GF and GF-PDMS Composite. First, Ni−F was dip-coated by GO of concentration 8 mg mL^{-1} with the assistance of vacuum. The GO-coated Ni−F was dried at 80 °C and put inside a 10% by weight (wt %) HI solution for 20 min for the reduction of GO to rGO. Later, the rGO-coated Ni−F was immersed in 3 M hot HCl solution at 80 °C for 24 h in order to ensure the complete removal of nickel. The pure GF was then dried at 80 °C for 2 h. Finally, PDMS was infused inside the GF via vacuum infiltration and cured at 80 °C.

Mechanical Tests. Mechanical tests were carried out using an Instron Model 5848 microtester. GF and GF-PDMS samples were tested first in quasi-static compression and subsequently cyclically in compression. Specimen dimensions used for GF were 5 mm × 4 mm × 3 mm. The specimen dimensions used for GF-PDMS composite were 10 mm (length), 8 mm (width), and 3 mm (thickness). The displacement-controlled static loading was carried out at a displacement rate of 1 mm min^{-1}, while the cyclic loading was carried out at a displacement rate of 30 mm min^{-1}. A 10 N load cell was used to test the mechanical properties of the GF, whereas a 2 kN load cell was used to test the GF-PDMS composite. In addition, a three-point bend test of the composite was done on samples with dimensions of 20 mm (length), 8 mm (width), and 3 mm (thickness) at a crosshead rate of 30 mm min^{-1}.

Change in Resistance Measurement. An oscilloscope (NI ELVIS II+ 100 MS/s) was coupled with the Instron Model 5848 microtester and the *in situ* change in resistance was measured during mechanical testing of the GF-PDMS composites.

Scanning Electron Microscopy, Energy-Dispersive Spectroscopy (EDS), and Raman Spectra. Scanning electron microscopy (SEM) (JEOL, Model JSM-7610F) was used for microstructural and EDS studies, while a spectrometer with a backscattered confocal configuration (Jobin Yvon Horiba, LabRAM), using a HeNe laser (633 nm), was employed for Raman characterization of GO and GF.

RESULTS AND DISCUSSION

The fabrication process of GF formation is shown schematically in Figure 1. The Ni−F is shown as a greenish skeleton, and the GO-coated Ni−F is shown in the subsequent step where the brownish red linings indicated the GO-coated Ni−F skeleton. A photograph of GF is shown in Figure 2e. EDS results verify the complete removal of nickel (see Figure S1b in the Supporting Information); >95% carbon, along with some oxygen, is indicated by the EDS peaks. In addition, the Raman spectra demonstrate the D- and G-band shifts of carbon at 1340 and 1570 cm^{-1}, as shown in Figure S1c in the Supporting Information. Based on a batch of five samples, GF has a density of 5.5 ± 1.3 mg cm^{-3}, estimated by measuring the volume and mass of the GF.

In order to understand and analyze the structure of the free-standing GF and its conformity with its Ni−F scaffold, SEM micrographs of the Ni−F and GF were taken at different resolutions. The SEM micrograph of pure GF shown in Figure 2b conforms well to the Ni−F shown in Figure 2a. The pore sizes of the Ni−F and the GF range between 100 mm and 400 mm.

DOI: 10.1021/acsami.5b01608
ACS Appl. Mater. Interfaces 2015, 7, 9195−9202

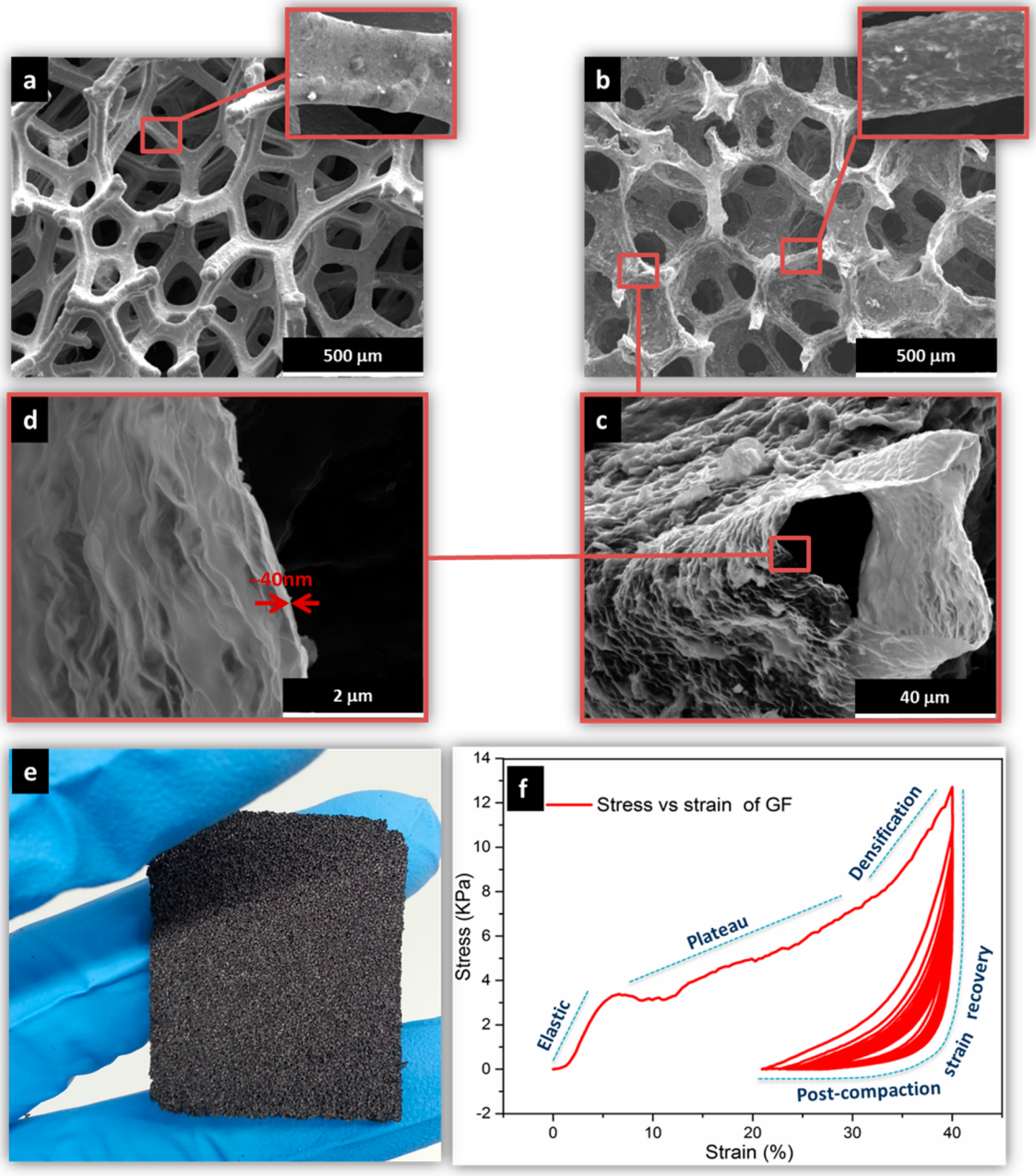

Figure 2. SEM micrographs of (a) Ni−F, (b) GF, (c) a close-up view of a single hollow bone of pure GF, and (d) the cross-sectional view of the wall of a single bone of the pure GF. Also shown are (e) a photograph of a free-standing pure GF sample and (f) a stress−strain curve of a GF sample.

The close-up micrographs of the single bones of GF and Ni−F appear to be different, as shown as insets in Figures 2a and 2b. The morphology of a single Ni−F bone appears compact and granular.[34] On the other hand, the surface morphology of a single bone of GF demonstrates a wrinkled structure of the layer-by-layer deposited rGO sheets, shown as an inset in Figure 2b. Since nickel has been completely removed from the core of the GF, the fractured top-view of a single GF bone is hollow, with very thin outer walls, as seen in Figure 2c. The wrinkled morphology of the surface of GF bone can also be seen clearly. A cross-sectional top-view image of the wall of GF bone shows a wall thickness of ∼40 nm (Figure 2d). In addition to understanding the morphology of a novel material, it is also imperative to recognize its mechanical behavior before analyzing its performance for load-bearing applications.

Cellular and porous foam materials have a generic mechanical behavior under quasi-static compressive loads. On their stress−strain curves, usually, there is an elasticity region at low stress, followed by a long collapse plateau, and it is then truncated by a densification region, whereby the stress rises steeply.[35] A typical stress−strain curve of GF is shown in Figure 2f. The GF monoliths behave like a typical elastic-brittle foam in compression, such as mullite (a ceramic foam), with a linear elasticity region, plateau, and densification regimes.[35] The elastic region is the response of individual bones and bone walls of the GF prior to the occurrence of any damage. The plateau region is due to the progressive failure of GF bones and bone walls. As more and more cells become crushed under compression, opposing GF bones and bone walls touch each other in compaction, leading to the final densification region.

DOI: 10.1021/acsami.5b01608
ACS Appl. Mater. Interfaces 2015, 7, 9195−9202

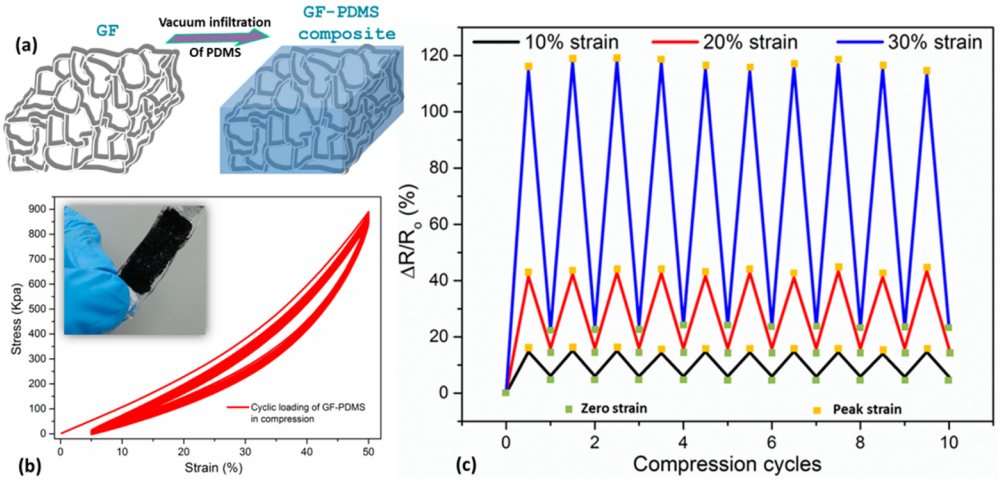

Figure 3. (a) Schematic representation of PDMS infusion inside pure GF; (b) cyclic stress−strain curve of a GF-PDMS composite, along with a photograph of GF-PDMS composite (inset); and (c) change in resistance of the composite with applied compressive cycles.

Densification occurs relatively rapidly with a steep rise in stress, as shown in the stress−strain curve.

Based on five samples of dimensions 3 mm × 4 mm × 5 mm, the elastic modulus is 89 ± 6 kPa. Additional stress−strain curves from different GF samples are shown in Figure S2 of the Supporting Information. When the load is released at 40% strain, almost 20% ± 5% of the strain is recovered and the sample displays somewhat elastic behavior when loaded repeatedly under compression. After 30 load cycles, the recovered strain is still ∼15% ± 5% based on a batch of five samples. This behavior is labeled as the post-compaction strain recovery in Figure 2f. The measured elastic moduli of GF are on the lower side when compared with other foams and similar structures. Nonetheless, this mechanical weakness becomes strength when it comes to its pressure sensing. The fact that the bones of GF undergo deformation at very low pressures and its electrical resistance changes simultaneously creates an opportunity of exploiting pressure-sensing behavior.

Flexible and stretchable electronics is an emerging field which requires flexible composite materials with both reliable mechanical integrity and suitable electrical conductivity.[36,37] Therefore, in order to induce robustness, strength, flexibility, and stretch-ability to the GF without compromising its change in electrical resistance upon deformation, PDMS was infiltrated in GF via a vacuum infusion method. The process of infusion is shown schematically in Figure 3a, and a photograph of the GF-PDMS composite with aluminum foil electrical connections are shown in the inset of Figure 3b. The GF-PDMS composites were examined for their mechanical integrity using a microtester. Loading−unloading compression cycles Nos. 1−500 of the GF-PDMS are shown in Figure 3b, where the hysteresis is almost the same, indicating that no substantial internal structural change has occurred. The slightly different behavior in the first loading−unloading cycle is usually observed in all elastomers.[38]

In order to quantify the change in electical resistance of the GF-PDMS composite in response to external stimuli such as pressure, an impedance measurement device was coupled with the microtester, and its electrical resistance was measured while deforming the composite under cyclic compressive loading. Change in resistance of the composite at strains of 10%, 20%, and 30% are shown in Figure 3c. The green squares show the relative change in resistance when the strain is zero, and the yellow squares show the relative change in resistance when the strain is in its peak value (i.e., 10%, 20%, or 30%). The resistance of the composite changes by 17% of the original value when compressed by 10%. Just like the case of stress−strain behavior, the change in electrical resistance of the first cycle is different from subsequent cycles, whereby it becomes more or less constant after the first cycle. The irreversible change in resistance after the first cycle may be due to the partial breaking or cracking of the GF bones. When increasing the compressive strain from 10% to 20%, the change in resistance increases from zero to ∼42%. For a compressive strain of 30%, the resistance changes to ∼120% of its original value. The irreversible part of the change in resistance in the first cycle becomes higher with higher amounts of strains induced in the composite, because of the permanent breakage or cracking of more GF bones than the lower strain values. The change in resistance at 30% compressive strain is repeated for ∼500 cycles, as shown in Figure S3 in the Supporting Information, demonstrating excellent electromechanical integrity, in terms of both stability and repeatibility of the GF-PDMS composite. In addition, the composite was twisted at 180° for at least 100 times, and it was tested for its change in resistance at 10% compressive strain, as shown in Figure S4 in the Supporting Information. The changes in resistance with compressive strain curves for both twisted and untwisted specimens correspond well with each other. These results reveal that the composite is rugged under shearing stresses as well, and its performance remains unperturbed by repeatly twisting it many times.

The GF-PDMS composite demonstrates a relative change in its electrical resistance when an external stimulus such as pressure is applied on it. However, this change is not linear for all pressure and load ranges. The relative change in resistance with pressures was investigated, as shown later in this work in Figure 5. The main curve relates the relative changes in resistance ($\Delta R/R_0$) with pressures ranging from 0 to ∼1300 kPa. Within this range, $\Delta R/R_0$ increases exponentially after 900 kPa and reaches 80 000%, becoming an insulator at 1300 kPa. Although the resistance changes significantly after 900 kPa, it does not imply that it changes linearly in the lower pressure range. A closeup of the main curve is shown as an inset, indicating a perfectly linear region until ∼230 kPa, and after which the curve becomes slightly nonlinear until 500 kPa. When a GF-PDMS composite sample connected to a light-emitting diode (LED) via a power supply is pressed, the illumination from the LED dims,

DOI: 10.1021/acsami.5b01608
ACS Appl. Mater. Interfaces 2015, 7, 9195−9202

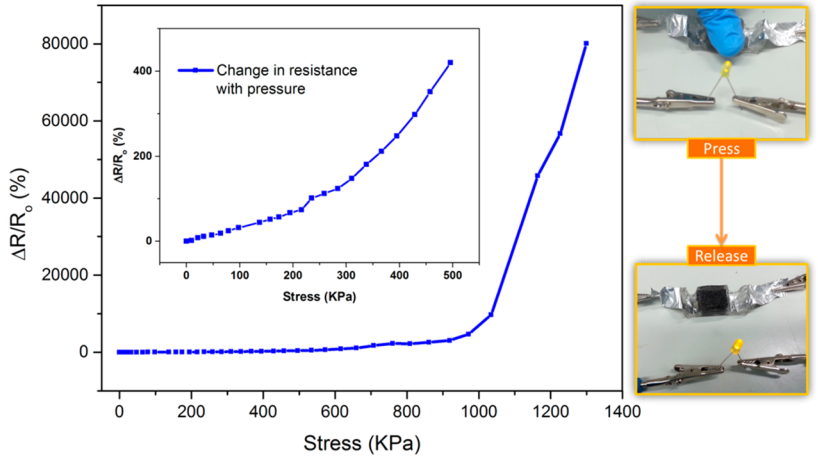

Figure 4. Relative change in electrical resistance of the GF-PDMS composite with applied static compressive loading, along with photographs of LED dimming and lighting up upon being pressed and released, respectively. Line connecting data only indicates the trend in the data.

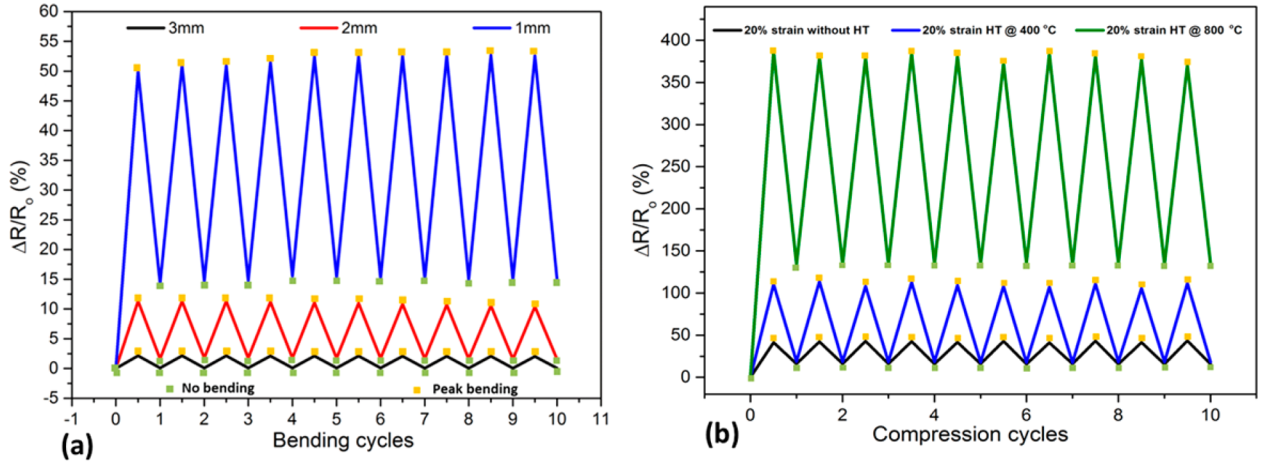

Figure 5. (a) Change in electrical resistance of GF-PDMS composite with different applied bending strains (bending radii); (b) effect of GF heat treatment on pressure sensitivity of GF-PDMS composite.

as shown in Figure 4. GF-PDMS composite possesses different sensitivity to the applied pressure at different pressure ranges. For instance, within the linear region of the inset of Figure 4 (i.e., pressure range 0−200 kPa), the sensitivity (defined as $\Delta R/R_0$/applied pressure, where $\Delta R/R_0$ is expressed as a percentage) is ∼0.6 kPa^{-1}, whereas it is ∼0.8 kPa^{-1} from 200 kPa to 500 kPa. In the exponential region of Figure 4, the sensitivity escalates to 60 kPa^{-1}.

In addition to testing and quantifying of strain and pressure sensitivity of the GF-PDMS composite in compression, its sensitivity in bending was also studied for three different bend radii of, 3, 2, and 1 mm (using sample with dimensions of 20 mm × 8 mm × 3 mm), results are shown in Figure 5. A material in bending undergoes different microstructural deformations than in compression; therefore, it can be envisaged that the pressure/strain sensitivity of the composite will be different in bending than that of the compression. In contrast to the stress in compression, which is given as force divided by cross-sectional area, the flexural stress at the midpoint of the composite (σ_f), under three-point bending load, is estimated by

$$\sigma_f = \frac{2P}{3bd^2}$$

where P is the applied load and b and d are the width and depth of the rectangular GF-PDMS composite, respectively. A cyclic bend radius of 3 mm, with a corresponding σ_f value of ∼0.93 MPa, produces a $\Delta R/R_0$ value of only ∼2.1%. A bend radius of 2 mm, with a corresponding σ_f value of ∼2.3 MPa, changes the resistance of the composite to ∼12%. Similarly, a rather bigger bend, with a radius of 1 mm and with a corresponding σ_f value of ∼5.6 MPa, produces a $\Delta R/R_0$ value of ∼52%. Just like the case of compression, the change in resistance due to bending also does not return to zero after the first cycle and remains constant during the rest of the bending cycles. The reason for the irreversible change in resistance in the first cycle could be attributed to the reasons discussed earlier.

For a pressure or strain sensor to be implemented successfully in low- and high-pressure-sensing applications, it should possess a tunable pressure sensing capability. GF were heat-treated at temperatures of 400 and 800 °C, and its effect on the sensitivity of the GF-PDMS composite was investigated. A plot of $\Delta R/R_0$, as a function of a 20% compressive strain, for untreated and heat-treated samples are shown in Figure 5b. As mentioned previously, a 20% compressive strain causes an ∼42% of change in the electrical resistance of the composite. However, heat-treating the composite at 400 °C results in a

DOI: 10.1021/acsami.5b01608
ACS Appl. Mater. Interfaces 2015, 7, 9195−9202

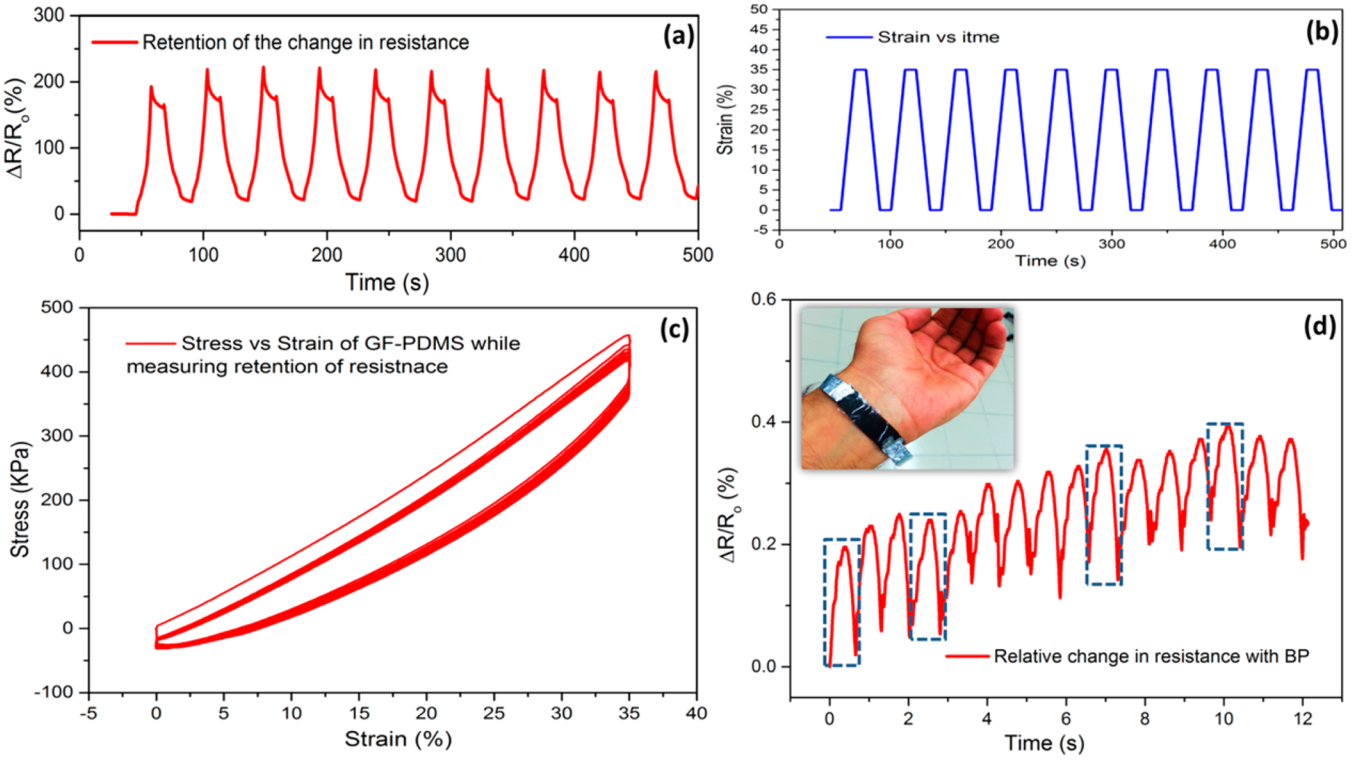

Figure 6. (a) Compressive strain versus time curve with strain being maintained at 0% and 35% for 10 s each; (b) the simultaneously taken cyclic stress−strain curve; (c) the simultaneously taken values of the relative change in resistance as a function of applied compressive strain; and (d) the blood pressure (BP) response of the GF-PDMS composite when in contact with a human wrist, in terms of the relative change in resistance.

$\Delta R/R_0$ value of ∼130% under the same compressive strain. The recorded $\Delta R/R_0$ value for the composite heat-treated at 800 °C, is ∼380%. Thus, heat treatment causes considerable change in the strain/pressure sensitivity of the composite, because it causes better reduction of the unreduced GO, as discussed elsewhere.[23,39−41] These results show that the strain/pressure sensitivity of the GF-PDMS composite can be tuned to a desired value by heat treating the GF at different temperatures.

In addition to probing the cyclic change in resistance with cyclically applied compressive or bending load, it is also important to know whether the change in resistance remains constant after longer term loading. This is studied by maintaining a 35% strain and 0% strain on the composite, in compression, for 10 s each, as shown in Figures 6a and 6b. A lower displacement rate of 5 mm min^{-1} was employed for this analysis, in order to avoid abrupt changes in resistance when the load is applied or removed. The curve depicted in the plot of strain versus time (Figure 6b) shows the crests and troughs of zero and 35% strain and the extent to which these strains are upheld. The cyclic stress−strain curve is shown in Figure 6b, showing some different behavior when compared to Figure 3c where strain is not upheld. When a 35% strain is maintained for 10 s, the stress relaxes from ∼380 kPa to ∼330 kPa, because of the viscoelastic behavior of the PDMS. The changes in resistance, taken simultaneously, are plotted in Figure 6c. The curve for the change in resistance with time corresponds reasonably well with the strain−time curve, with a slight decrease in $\Delta R/R_0$ at a peak strain of 35%. At this peak strain, $\Delta R/R_0$ reaches a value of ∼200%, which decreases to ∼10% in 10 s. This decrease in $\Delta R/R_0$ is associated with the drop in the stress at peak strain due to the viscoelastic slackening of the GF-PDMS composite, as observed in Figure 6b. Therefore, from these results, it can be concluded that the resistance of the composite corresponds well to the applied strain and the change caused by a certain strain in the composite remains static if the applied strain is maintained.

Considering the enhanced pressure/strain sensitivity of the GF-PDMS composite with GF heat-treated at 800 °C, the composite was used to sense human blood pressure (BP). The composite was attached to the wrist of a volunteer, and the relative change in electrical resistance, relative to time, was measured, as shown in Figure 6d. The pulses are shown as the crests and troughs of the relative change in resistance peaks. The cyclic curve for BP measurement shows pulse peaks of about equal strength. The randomly picked pulse peaks, denoted by dotted lines in Figure 6d, show the strength of each peak, which is ∼0.2% ± 1 standard deviation. Upon calibration of these results, the BP can be measured within 1 s. Since the blood pulses in veins are associated with the heartbeat rate, this composite sensor can also be used to monitor the heartbeat rate. In addition, the composite may potentially be used as a respirometer.

CONCLUSIONS

We have successfully mimicked the Ni−F structure into a free-standing three-dimensional (3D) graphene foam (GF) via a facile dip-coating, reduction, and etching method. The resulting GF possesses the typical fracture behavior of elastic-brittle foam with an elastic modulus of ∼89 kPa. Vacuum infusion of PDMS into GF results in a resilient and flexible composite. When tested in cyclic compressive loading, it changes its electrical resistance. Upon the application of a compressive strain of 30% on the GF-PDMS composite, its resistance increases to ∼120% of its original value. Similarly, bending a sample to a radius of 1 mm causes the composite to change its resistance to ∼52% of

DOI: 10.1021/acsami.5b01608
ACS Appl. Mater. Interfaces 2015, 7, 9195−9202

its original resistance value. The composite changes its resistance linearly with applied compressive stresses of up to 200 kPa and becomes slightly nonlinear until an applied pressure of 500 kPa and later changes fairly exponentially. When heat treating the GF at 800 °C prior to PDMS infusion, the GF-PDMS demonstrates ~10 times better sensitivity than the untreated sample for a compressive strain of 20%. The composite was also demonstrated to record human blood pressure and heartbeat rate.

■ ASSOCIATED CONTENT

Supporting Information

The Supporting Information includes the EDS data and Raman spectra and stress versus strain curves under compression load for the GF. It also includes the $\Delta R/R_0$ of GF-PDMS composite at a compressive cycle strain of 30% for 500 cycles and comparison in the $\Delta R/R_0$ of GF-PDMS composite before and after twisting 100 times. Supporting Information also includes an SEM micrograph of pure GF, EDS data for pure GF, Raman spectra of pure GF, stress−strain curves for three samples of GF, change in resistance as a function of applied 30% cyclic strain for 500 cycles, and the effect of twisting on the change in resistance of GF-PDMS composite and the SEM micrographs of pre-fracture and post-fracture GF. This material is available free of charge via the Internet at http://pubs.acs.org.

■ AUTHOR INFORMATION

Corresponding Author

*Tel.: +971-(0)2-5018583. E-mail: kin.liao@kustar.ac.ae.

Author Contributions

§The manuscript was written through contributions of all authors. These authors contributed equally.

Funding

This work was funded by the Mechanical Engineering Department of Khalifa University of Science Technology and Research.

Notes

The authors declare no competing financial interest.

■ ACKNOWLEDGMENTS

The authors would like to thank Prof. Lianxi Zheng for his intellectual discussion on the topic.

■ REFERENCES

(1) Kolata, G. How can Computers get Common Sense? *Science* **1982**, *217*, 1237−1238.
(2) Rogers, J. A.; Someya, T.; Huang, Y. Materials and Mechanics for Stretchable Electronics. *Science* **2010**, *327*, 1603−1607.
(3) Gardner, J. W.; Bartlett, P. N. A Brief History of Electronic Noses. *Sens. Actuators, B* **1994**, *18*, 210−211.
(4) Favier, F.; Walter, E. C.; Zach, M. P.; Benter, T.; Penner, R. M. Hydrogen Sensors and Switches from Electrodeposited Palladium Mesowire Arrays. *Science* **2001**, *293*, 2227−2231.
(5) Boland, J. J. Flexible Electronics: Within Touch of Artificial Skin. *Nat. Mater.* **2010**, *9*, 790−792.
(6) Mannsfeld, S. C.; Tee, B. C.; Stoltenberg, R. M.; Chen, C. V. H.; Barman, S.; Muir, B. V.; Sokolov, A. N.; Reese, C.; Bao, Z. Highly Sensitive Flexible Pressure Sensors with Microstructured Rubber Dielectric Layers. *Nat. Mater.* **2010**, *9*, 859−864.
(7) Takei, K.; Takahashi, T.; Ho, J. C.; Ko, H.; Gillies, A. G.; Leu, P. W.; Fearing, R. S.; Javey, A. Nanowire Active-matrix Circuitry for Low-voltage Macroscale Artificial Skin. *Nat. Mater.* **2010**, *9*, 821−826.
(8) Mills, D. A.; Alexander, D.; Subhash, G.; Sheplak, M. In Development of a sapphire optical pressure sensor for high-temperature applications, SPIE Sensing Technology + Applications. *Int. Soc. Opt. Photonics* **2014**, 91130H-1−91130H-15.
(9) Shao, Q.; Niu, Z.; Hirtz, M.; Jiang, L.; Liu, Y.; Wang, Z.; Chen, X. High-Performance and Tailorable Pressure Sensor Based on Ultrathin Conductive Polymer Film. *Small* **2014**, *10*, 1466−1472.
(10) Jung, S.; Kim, J. H.; Kim, J.; Choi, S.; Lee, J.; Park, I.; Hyeon, T.; Kim, D. H. Reverse-Micelle-Induced Porous Pressure-Sensitive Rubber for Wearable Human−Machine Interfaces. *Adv. Mater.* **2014**, *26*, 4825−4830.
(11) Eda, G.; Fanchini, G.; Chhowalla, M. Large-area Ultrathin Films of Reduced Graphene Oxide as a Transparent and Flexible Electronic Material. *Nat. Nanotechnol.* **2008**, *3*, 270−274.
(12) Kim, K. S.; Zhao, Y.; Jang, H.; Lee, S. Y.; Kim, J. M.; Kim, K. S.; Ahn, J.-H.; Kim, P.; Choi, J.-Y.; Hong, B. H. Large-scale Pattern Growth of Graphene Films for Stretchable Transparent Electrodes. *Nature* **2009**, *457*, 706−710.
(13) Bonaccorso, F.; Sun, Z.; Hasan, T.; Ferrari, A. Graphene Photonics and Optoelectronics. *Nat. Photonics* **2010**, *4*, 611−622.
(14) Wu, Q.; Xu, Y.; Yao, Z.; Liu, A.; Shi, G. Supercapacitors Based on Flexible Graphene/Polyaniline Nanofiber Composite Films. *ACS Nano* **2010**, *4*, 1963−1970.
(15) Bunch, J. S.; Verbridge, S. S.; Alden, J. S.; van der Zande, A. M.; Parpia, J. M.; Craighead, H. G.; McEuen, P. L. Impermeable Atomic Membranes from Graphene Sheets. *Nano Lett.* **2008**, *8*, 2458−2462.
(16) Geim, A. K. Graphene: Status and Prospects. *Science* **2009**, *324*, 1530−1534.
(17) Geim, A. K.; Novoselov, K. S. The Rise of Graphene. *Nat. Mater.* **2007**, *6*, 183−191.
(18) Xu, Y.; Guo, Z.; Chen, H.; Yuan, Y.; Lou, J.; Lin, X.; Gao, H.; Chen, H.; Yu, B. In-plane and Tunneling Pressure Sensors Based on Graphene/Hexagonal Boron Nitride Heterostructures. *Appl. Phys. Lett.* **2011**, *99*, 133109.
(19) Dimitrakakis, G. K.; Tylianakis, E.; Froudakis, G. E. Pillared Graphene: A New 3-D Network Nanostructure for Enhanced Hydrogen Storage. *Nano Lett.* **2008**, *8*, 3166−3170.
(20) Chen, Z.; Ren, W.; Gao, L.; Liu, B.; Pei, S.; Cheng, H.-M. Three-dimensional Flexible and Conductive Interconnected Graphene Networks Grown by Chemical Vapour Deposition. *Nat. Mater.* **2011**, *10*, 424−428.
(21) Qiu, L.; Liu, J. Z.; Chang, S. L.; Wu, Y.; Li, D. Biomimetic Superelastic Graphene-Based Cellular Monoliths. *Nat. Commun.* **2012**, *3*, 1241.
(22) Worsley, M. A.; Kucheyev, S. O.; Mason, H. E.; Merrill, M. D.; Mayer, B. P.; Lewicki, J.; Valdez, C. A.; Suss, M. E.; Stadermann, M.; Pauzauskie, P. J.; Satcher, J. H.; Biener, J.; Baumann, T. F. Mechanically Robust 3D Graphene Macroassembly with High Surface Area. *Chem. Commun.* **2012**, *48*, 8428−8430.
(23) Worsley, M. A.; Pham, T. T.; Yan, A.; Shin, S. J.; Lee, J. R. I.; Bagge-Hansen, M.; Mickelson, W.; Zettl, A. Synthesis and Characterization of Highly Crystalline Graphene Aerogels. *ACS Nano* **2014**, *8* (10), 11013−11022.
(24) Xu, Y.; Sheng, K.; Li, C.; Shi, G. Self-Assembled Graphene Hydrogel via a One-Step Hydrothermal Process. *ACS Nano* **2010**, *4* (7), 4324−4330.
(25) Xia, Z. Y.; Wei, D.; Anitowska, E.; Bellani, V.; Ortolani, L.; Morandi, V.; Gazzano, M.; Zanelli, A.; Borini, S.; Palermo, V. Electrochemically Exfoliated Graphene Oxide/Iron Oxide Composite Foams for Lithium Storage, Produced by Simultaneous Graphene Reduction and $Fe(OH)_3$ Condensation. *Carbon* **2014**, *84*, 254−262.
(26) Yazyev, O. V.; Louie, S. G. Electronic Transport in Polycrystalline Graphene. *Nat. Mater.* **2010**, *9*, 806−809.
(27) Samad, Y. A.; Li, Y.; Schiffer, A.; Alhassan, S. M.; Liao, K. Graphene Foam Developed with a Novel Two-Step Technique for Low and High Strains and Pressure-Sensing Applications. *Small* **2015**, DOI: 10.1002/smll.201403532.
(28) Li, Y.; Chen, J.; Huang, L.; Li, C.; Hong, J. D.; Shi, G. Highly Compressible Macroporous Graphene Monoliths via an Improved Hydrothermal Process. *Adv. Mater.* **2014**, *26*, 4789−4793.
(29) Yao, H. B.; Ge, J.; Wang, C. F.; Wang, X.; Hu, W.; Zheng, Z. J.; Ni, Y.; Yu, S. H. A Flexible and Highly Pressure-Sensitive Graphene−

DOI: 10.1021/acsami.5b01608
ACS Appl. Mater. Interfaces 2015, 7, 9195−9202

Polyurethane Sponge Based on Fractured Microstructure Design. *Adv. Mater.* **2013**, *25*, 6692−6698.
(30) Wu, C.; Fang, L.; Huang, X.; Jiang, P. Three-Dimensional Highly Conductive Graphene-Silver Nanowire Hybrid Foams for Flexible and Stretchable Conductors. *ACS Appl. Mater. Interfaces* **2014**, *6*, 21026−21034.
(31) Bansal, A. K.; Hou, S.; Kulyk, O.; Bowman, E. M.; Samuel, I. D. Wearable Organic Optoelectronic Sensors for Medicine. *Adv. Mater.* **2014**, DOI: 10.1002/adma.201403560.
(32) Li, Y.; Umer, R.; Samad, Y. A.; Zheng, L.; Liao, K. The Effect of the Ultrasonication Pre-treatment OF Graphene Oxide (GO) on the Mechanical Properties of GO/Polyvinyl Alcohol Composites. *Carbon* **2013**, *55*, 321−327.
(33) Li, D.; Muller, M. B.; Gilje, S.; Kaner, R. B.; Wallace, G. G. Processable Aqueous Dispersions of Graphene Nanosheets. *Nat. Nanotechnol.* **2008**, *3*, 101−105.
(34) Yuan, Y. F.; Xia, X. H.; Wu, J. B.; Yang, J. L.; Chen, Y. B.; Guo, S. Y. Nickel Foam-Supported Porous $Ni(OH)_2$/NiOOH Composite Film as Advanced Pseudocapacitor Material. *Electrochim. Acta* **2011**, *56*, 2627−2632.
(35) Gibson, L. J.; Ashby, M. F. *Cellular Solids: Structure and Properties*, Second Edition; Cambridge University Press: Cambridge, U.K., 1997; p 500.
(36) Service, R. F. Electronic Textiles Charge Ahead. *Science* **2003**, *301*, 909−911.
(37) Sekitani, T.; Noguchi, Y.; Hata, K.; Fukushima, T.; Aida, T.; Someya, T.; Rubberlike, A. Stretchable Active Matrix Using Elastic Conductors. *Science* **2008**, *321*, 1468−1472.
(38) Hou, C.; Czubernat, K.; Jin, S. Y.; Altenhof, W.; Maeva, E.; Seviaryna, I.; Bandyopadhyay-Ghosh, S.; Sain, M.; Gu, R. Mechanical Response of Hard Bio-based PU Foams under Cyclic Quasi-static Compressive Loading Conditions. *Int. J. Fatigue* **2014**, *59*, 76−89.
(39) Huang, Z.; Zhang, H.; Chen, Y.; Wang, W.; Chen, Y.; Zhong, Y. Microwave-Assisted Synthesis of Functionalized Graphene on Ni Foam as Electrodes for Supercapacitor Application. *Electrochim. Acta* **2013**, *108*, 421−428.
(40) Worsley, M. A.; Pauzauskie, P. J.; Olson, T. Y.; Biener, J.; Satcher, J. H., Jr.; Baumann, T. F. Synthesis of Graphene Aerogel with High Electrical Conductivity. *J. Am. Chem. Soc.* **2010**, *132*, 14067−14069.
(41) Xu, Z.; Zhang, Y.; Li, P.; Gao, C. Strong, Conductive, Lightweight, Neat Graphene Aerogel Fibers with Aligned Pores. *ACS Nano* **2012**, *6*, 7103−7113.

DOI: 10.1021/acsami.5b01608
ACS Appl. Mater. Interfaces 2015, 7, 9195−9202